AGU PUBLICATIONS

JGR

Journal of Geophysical Research: Atmospheres

RESEARCH ARTICLE
10.1002/2015JD024322

Key Points:
- LWP retrieval sensitivity to drizzle and cloud top entrainment is quantified using LES
- Suitable profile assumptions for retrieval are found to be related to cloud regime
- A modified adiabatic profile is developed to explain variability in LWP retrievals

Correspondence to:
D. J. Miller,
dj-miller@umbc.edu

Citation:
Miller, D. J., Z. Zhang, A. S. Ackerman, S. Platnick, and B. A. Baum (2016), The impact of cloud vertical profile on liquid water path retrieval based on the bispectral method: A theoretical study based on large-eddy simulations of shallow marine boundary layer clouds, *J. Geophys. Res. Atmos.*, *121*, 4122–4141, doi:10.1002/2015JD024322.

Received 9 OCT 2015
Accepted 20 MAR 2016
Accepted article online 6 APR 2016
Published online 25 APR 2016

The impact of cloud vertical profile on liquid water path retrieval based on the bispectral method: A theoretical study based on large-eddy simulations of shallow marine boundary layer clouds

Daniel J. Miller[1], Zhibo Zhang[1,2], Andrew S. Ackerman[3], Steven Platnick[4], and Bryan A. Baum[5]

[1]Physics Department, University of Maryland, Baltimore County, Baltimore, Maryland, USA, [2]Joint Center for Earth Systems Technology, Baltimore, Maryland, USA, [3]NASA Goddard Institute for Space Studies, New York, New York, USA, [4]NASA Goddard Space Flight Center, Greenbelt, Maryland, USA, [5]Space Science and Engineering Center, University of Wisconsin-Madison, Madison, Wisconsin, USA

Abstract Passive optical retrievals of cloud liquid water path (LWP), like those implemented for Moderate Resolution Imaging Spectroradiometer (MODIS), rely on cloud vertical profile assumptions to relate optical thickness (τ) and effective radius (r_e) retrievals to LWP. These techniques typically assume that shallow clouds are vertically homogeneous; however, an adiabatic cloud model is plausibly more realistic for shallow marine boundary layer cloud regimes. In this study a satellite retrieval simulator is used to perform MODIS-like satellite retrievals, which in turn are compared directly to the large-eddy simulation (LES) output. This satellite simulator creates a framework for rigorous quantification of the impact that vertical profile features have on LWP retrievals, and it accomplishes this while also avoiding sources of bias present in previous observational studies. The cloud vertical profiles from the LES are often more complex than either of the two standard assumptions, and the favored assumption was found to be sensitive to cloud regime (cumuliform/stratiform). Confirming previous studies, drizzle and cloud top entrainment of dry air are identified as physical features that bias LWP retrievals away from adiabatic and toward homogeneous assumptions. The mean bias induced by drizzle-influenced profiles was shown to be on the order of 5–10 g/m^2. In contrast, the influence of cloud top entrainment was found to be smaller by about a factor of 2. A theoretical framework is developed to explain variability in LWP retrievals by introducing modifications to the adiabatic r_e profile. In addition to analyzing bispectral retrievals, we also compare results with the vertical profile sensitivity of passive polarimetric retrieval techniques.

1. Introduction

Cloud liquid water path (LWP) is a key parameter in many cloud physical processes (e.g., condensation, evaporation, and precipitation) and largely determines cloud shortwave radiative forcing. Many techniques have been developed to retrieve cloud LWP from satellite observations. In this study, we focus on the so-called bispectral solar reflectance method (hereafter "bispectral method") of *Nakajima and King* [1990]. This method employs a pair of cloud reflection observations, one in the visible and near-infrared (VNIR), and the other in the shortwave-infrared (SWIR) spectral region. These two bands are used to simultaneously retrieve cloud optical thickness (τ) and cloud droplet effective radius (r_e). Cloud LWP can be computed from the retrieved τ and r_e by using the relationship,

$$\mathrm{LWP} = C\rho_l r_e \tau, \tag{1}$$

where ρ_l is the bulk density of liquid water and C is a coefficient that can be derived from the assumed vertical cloud profile (see section 2 for more discussion). Several widely used satellite cloud property products are based on the bispectral method. Most notably, this includes the operational cloud products from the Moderate Resolution Imaging Spectroradiometer (MODIS) [*King et al.*, 2003; *Platnick et al.*, 2003], the Spinning Enhanced Visible and Infrared Imager (SEVIRI) [*Roebeling et al.*, 2006], and National Polar-orbiting Partnership Visible Infrared Imaging Radiometer Suite (NPP VIIRS) [*Rosenfeld et al.*, 2014]. The cloud products derived from these instruments include LWP retrievals used in numerous studies, for example, to evaluate spatial variability of MBL cloud LWP [*Wood and Hartmann*, 2006], to study the warm rain process in MBL clouds [*Kubar and Hartmann*, 2009; *Suzuki et al.*, 2011], to evaluate cloud LWP simulation in climate models [*Jiang et al.*, 2012], and to assess the impact of aerosols on MBL clouds [*Costantino and Breon*, 2013].

The wide use of the bispectral method makes it important to understand its inherent limitations and potential sources of retrieval uncertainty. Among others, the influence of cloud vertical profile on the bispectral retrieval of LWP has received significant and increasing attention in recent years [*Wood and Hartmann*, 2006; *Bennartz*, 2007; *Seethala and Horváth*, 2010; *Lebsock and Su*, 2014]. In operational bispectral retrieval algorithms, clouds are commonly assumed to be vertically homogeneous (i.e., $r_e(\tau)$ is constant) which implies that the constant $C = 2/3$ in equation (1), and thus,

$$\mathrm{LWP}_h = \frac{2}{3}\rho_l r_e \tau. \tag{2}$$

Here the subscript "*h*" denotes LWP retrievals based on the homogeneous vertical profile assumption. It is well established, however, that MBL clouds may develop inhomogeneous vertical profiles as a result of a variety of physical processes. For example, in situ measurements commonly resemble an adiabatic profile associated with droplet condensational growth in nonprecipitating MBL clouds. Adiabatic profiles exhibit cloud water content (LWC) that increases linearly with height from cloud base, because cloud droplet number concentration (CDNC) is constant and all droplet activation occurs at the cloud base [*Nicholls and Leighton*, 1986; *Miles et al*., 2000; *Brenguier et al*., 2003]. In situ observations of MBL clouds typically differ slightly from the theoretical adiabatic profile, with a reduced vertical gradient of LWC compared to theory. Profiles exhibiting this reduced gradient are referred to as subadiabatic. On the basis of these observations, a number of recent studies have argued that an adiabatic or subadiabatic profile is a better assumption for LWP retrievals. These studies have also suggested that assuming clouds to be vertically homogeneous could lead to overestimation of the LWP of MBL clouds [*Wood and Hartmann*, 2006; *Seethala and Horváth*, 2010]. For both adiabatic and subadiabatic vertical profiles $C = 5/9$ in equation (1) leading to the expression:

$$\mathrm{LWP}_{\mathrm{ad}} = \frac{5}{9}\rho_l r_e^{\mathrm{top}} \tau, \tag{3}$$

where r_e^{top} specifically denotes the droplet size at cloud top and the subscript "ad" denotes the assumption of adiabatic or subadiabatic vertical profile. In an operational retrieval sense, where the same droplet size retrieval may be used for both LWP_h and $\mathrm{LWP}_{\mathrm{ad}}$ assumptions, the difference between equations (2) and (3) is purely in terms of the value of the constant *C*. Given that both adiabatic and subadiabatic behavior result in the same LWP relationship, we will simply refer to this as the "adiabatic" LWP relationship.

Although the adiabatic profile is more appealing and has been increasingly favored over the homogeneous profile in recent studies, only a few have systematically compared and evaluated LWP retrievals based on the two assumptions. For example, *Seethala and Horváth* [2010] compared the two sets of MODIS LWP retrievals (LWP_h and $\mathrm{LWP}_{\mathrm{ad}}$) with collocated LWP retrievals from the Advanced Microwave Scanning Radiometer for EOS (AMSR-E). One advantage of the AMSR-E retrieval is that it is less sensitive to cloud vertical profile because the information content for the retrieval comes from transmitted surface microwave emission. Interestingly, they found that assuming adiabatic vertical profile in MODIS LWP retrievals does not always lead to a better agreement with AMSR-E results (see their Figure 6). Over the subtropical coastal stratocumulus regions (e.g., SE Atlantic and Pacific), the results are as expected: the LWP_h overestimates AMSR-E retrievals and the retrieval assuming adiabatic profile, $\mathrm{LWP}_{\mathrm{ad}}$, leads to better agreement between the two instruments. However, over tropical and subtropical shallow cumulus regions, the adiabatic assumption increases the difference between the two methods. The LWP_h retrievals from MODIS over these regions are already smaller than AMSR-E results, and assuming an adiabatic profile, $\mathrm{LWP}_{\mathrm{ad}}$, makes the underestimation bias even worse. The authors listed a number of potential issues in both MODIS and AMSR-E retrieval techniques that may cause such a bias. However, one possible physical explanation they noted was that entrainment of dry air at cloud top can reduce r_e and thereby induce an underestimated LWP. This occurs because MODIS r_e retrievals are particularly sensitive to cloud top properties. In a more recent study, *Lebsock and Su* [2014] carried out a comprehensive intercomparison between MODIS (based on adiabatic $\mathrm{LWP}_{\mathrm{ad}}$), AMSR-E, and CloudSat LWP retrievals over global oceans. Similar to Seethala and Horváth, they also found that MODIS $\mathrm{LWP}_{\mathrm{ad}}$ retrievals are in better agreement with the other two data sets over subtropical stratocumulus regions than over tropical and subtropical cumulus cloud regions. Taking advantage of the sensitivity of the CloudSat radar to precipitation in MBL clouds, they found that over the subtropical cumulus cloud regions rainwater accounts for a substantial portion of LWP (see their Figure 14). They hypothesized that the LWP retrieval differences between MODIS and AMSR-E over these regions may be partly caused by

differences in the sensitivity of MODIS and AMSR-E algorithms to precipitation. In addition to remote sensing studies, MODIS LWP retrievals have also been rigorously compared to in situ observations in field campaigns specifically examining MBL clouds (stratocumulus) [*Noble and Hudson*, 2015]. This study indicated several potential sources of bias for r_e and τ that propagate into LWP retrievals. Comparing the homogeneous and adiabatic retrieval assumptions to the in situ observations led to mean LWP retrieval biases of 37% and 14%, respectively. For one of the in situ data sets studied the MODIS retrieval of τ did not appear to be the source of LWP bias, while r_e retrievals were found to be high biased despite being well correlated with in situ measurements. One of the conclusions of *Noble and Hudson* [2015] was that MODIS captured the variability of r_e while still being systematically biased due to cloud inhomogeneity, cloud top retrieval sensitivity, or temporal discrepancies between in situ cloud penetration and satellite overpass.

These recent studies have shed light on important limitations and uncertainties associated with bispectral LWP retrievals in comparison with other remote sensing techniques. Beyond cloud vertical profile, however, the bispectral method is sensitive to other sources of retrieval bias. Notable examples include inhomogeneous cloud horizontal structure and retrieval resolution [*Oreopoulos and Davies*, 1998; *Zhang et al*., 2012], as well as 3-D radiative transfer effects [*Várnai and Davies*, 1999; *Várnai and Marshak*, 2001, 2002; *Marshak et al*., 2006]. These sensitivities are often entangled such that it is problematic to completely separate them in observational studies like those previously mentioned. Moreover, the physical mechanisms underlying the influence of cloud vertical profile on the bispectral LWP retrieval remain largely unexplored in the observational studies.

This study approaches the problem from a different perspective; rather than use remote sensing data, synthetic retrievals are generated from large-eddy simulations (LESs) of cloud scenes. Synthetic retrievals are obtained by modeling the radiative transfer of a scene and performing bispectral retrievals using the resulting reflectances. As discussed in detail in section 3, an advantage of using synthetic retrievals is that uncertainty sources in the retrieval are known and can be controlled, permitting a more focused and in-depth study. The overall objective is to improve understanding of how cloud vertical profile affects bispectral LWP retrievals. More specifically, we hope to shed light on three questions. First, which cloud vertical profile assumption, homogeneous (LWP_h), or adiabatic (LWP_{ad}), leads to bispectral LWP retrievals that agree better with the "ground truth" from our LES cases? Second, how does cloud vertical profile vary with MBL cloud types (e.g., stratocumulus versus cumulus) and what are the consequences of selecting a particular cloud vertical profile assumption for bispectral retrievals? Third, how do cloud top entrainment and the presence of drizzle in MBL clouds influence bispectral retrievals? We address these questions not only using numerical simulations but also by developing a theoretical and analytical framework that can explain the bispectral LWP retrievals for a given "true" cloud vertical profile from the LES cloud model.

2. Theoretical Basis

Cloud LWP is defined as the column-integrated cloud liquid water content from cloud base to cloud top:

$$\mathrm{LWP} = \rho_l \int_{Z_{\mathrm{base}}}^{Z_{\mathrm{top}}} \int_0^\infty \frac{4}{3}\pi r^3 N(r,z)\mathrm{d}r \ \mathrm{d}z, \tag{4}$$

where $N(r,z)$ is the cloud droplet size distribution at level z. The vertical dimension of the above integral can be converted to optical thickness space, which is more relevant to the bispectral method:

$$\mathrm{LWP} = \frac{4}{3}\frac{\rho_l}{Q_e}\int_0^{\tau_{\mathrm{tot}}} r_e(\tau)\mathrm{d}\tau \approx \frac{2}{3}\rho_l \int_0^{\tau_{\mathrm{tot}}} r_e(\tau)\mathrm{d}\tau, \tag{5}$$

where Q_e is the extinction coefficient; τ_{tot} is the total cloud optical thickness in the visible region, where $Q_e \approx 2$; and $r_e(\tau)$ is defined as follows:

$$r_e(\tau) = \frac{\int_0^\infty r^3 N(r,\tau)\mathrm{d}r}{\int_0^\infty r^2 N(r,\tau)\mathrm{d}r}. \tag{6}$$

It should be clarified that $\tau = 0$ is at cloud top (Z_{top}) and $\tau = \tau_{\mathrm{tot}}$ at cloud base (Z_{base}). In the conversion we have made use of the relationship between the optical depth and the extinction cross section, $\sigma_e(z) = \mathrm{d}\tau/\mathrm{d}z = Q_e \pi \int_0^\infty r^2 N(r,z)\mathrm{d}r$.

As far as vertical profile is concerned, the bispectral retrieval of LWP faces two major challenges. The first is that the vertical profile of cloud microphysics (i.e., $N(r,\tau)$ and $r_e(\tau)$) are unknown prior to the retrieval although they could have a significant impact on the outcome. In practice, a priori assumptions are made to enable LWP retrieval from retrieved τ and r_e. In many operational retrieval algorithms, r_e is simply assumed to be a constant throughout the cloud, in which case the homogeneous $\mathrm{LWP}_h = \frac{2}{3}\rho_l r_e \tau$ is used. Another common assumption is that $r_e(\tau)$ follows the adiabatic growth model which leads to a power law relationship (see equation (35) for the explicit relationship) [*Pontikis*, 1996; *Szczodrak et al*., 2001]:

$$r_e(\tau) = r_e^{\mathrm{top}}\left(\frac{\tau_{\mathrm{tot}} - \tau}{\tau_{\mathrm{tot}}}\right)^{1/5}, \tag{7}$$

where r_e^{top} is the droplet effective radius at cloud top, i.e., $r_e^{\mathrm{top}} = r_e(\tau = 0)$. By substituting equation (7) into equation (5), one can obtain the adiabatic cloud LWP:

$$\mathrm{LWP}_{\mathrm{ad}} = \frac{2}{3}\rho_l \int_0^{\tau_{\mathrm{tot}}} r_e^{\mathrm{top}}\left(\frac{\tau_{\mathrm{tot}} - \tau}{\tau_{\mathrm{tot}}}\right)^{1/5} \mathrm{d}\tau = \frac{2}{3}\rho_l\left(\frac{5}{6} r_e^{\mathrm{top}} \tau_{\mathrm{tot}}\right) = \frac{5}{9}\rho_l r_e^{\mathrm{top}} \tau_{\mathrm{tot}}. \tag{8}$$

The second major challenge facing the bispectral retrieval is that the absorbing SWIR bands have only limited penetration depth into the cloud and as a result the retrieved r_e is weighted toward the microphysics prevalent in the upper part of the cloud [*Platnick*, 2000]. Therefore, an important step toward understanding the retrieval results is to understand the vertical weighting involved in the r_e retrieval. In this study, we focus on the r_e retrieval based on the 3.75 μm SWIR band for a few reasons. First, it is a common SWIR band found on board most passive polar-orbiting and geostationary instruments, such as advanced very high resolution radiometer, MODIS, VIIRS, and SEVIRI. Recent studies also indicate that the 3.75 μm band is less sensitive to 3-D radiative transfer effects than other SWIR bands, such as 2.13 and 1.65 μm [*Zhang and Platnick*, 2011; *Zhang et al*., 2012; *Cho et al*., 2015]. More importantly for this study, the strong absorption by cloud droplets in the 3.75 μm band makes it possible to approximate the cloud reflectance in this wavelength as being dominated by single scattering (i.e., multiple scattering is inhibited by absorption). As such, an analytical vertical weighting function ($W(\tau)$) can be approximated by a two-way transmittance (2WT) function as follows [*Platnick*, 2000; *Alexandrov et al*., 2012]:

$$u(\tau) = \exp\left[-\tau\left(\frac{1}{\mu_0} + \frac{1}{\mu_v}\right)\right], \tag{9}$$

$$W(\tau) \equiv \frac{1}{C}\frac{\mathrm{d}u}{\mathrm{d}\tau}, \tag{10}$$

$$\int_0^{\tau_{\mathrm{tot}}} W(\tau)\mathrm{d}\tau = 1, \tag{11}$$

where μ_0 and μ_v are the cosines of the solar and viewing zenith angles, respectively. The form of $u(\tau)$ corresponds to the attenuation of two-way transmittance and leads to the definition of the vertical weighting function $W(\tau)$. This vertical weighting function provides a useful tool for interpreting r_e retrievals and comparing them to the microphysical properties of the scene. In *Platnick* [2000], $W(\tau)$ is used to estimate r_e retrieval, $r_{e,W}$, from the vertical profile of $r_e(\tau)$,

$$r_{e,W} = \int_0^{\tau_{\mathrm{tot}}} r_e(\tau) W(\tau)\mathrm{d}\tau. \tag{12}$$

However, a different approach to vertical weighting is adopted in this study. As described by *Alexandrov et al*. [2012], the vertical weighting function $W(\tau)$ is first used to derive an effective size distribution, $N_{2\mathrm{WT}}$, which is an optically weighted superposition of the droplet size distributions throughout the cloud column.

$$N_{2\mathrm{WT}}(r) = \int_0^{\tau_{\mathrm{tot}}} N(r,\tau) W(\tau)\mathrm{d}\tau. \tag{13}$$

The effective size distribution $N_{2\mathrm{WT}}$ is then used to produce a vertically weighted r_e,

$$r_{e,\,2\mathrm{WT}} = \frac{\int_0^\infty r^3 N_{2\mathrm{WT}}(r)\mathrm{d}r}{\int_0^\infty r^2 N_{2\mathrm{WT}}(r)\mathrm{d}r}. \tag{14}$$

The advantage of first defining a vertically weighted droplet size distribution is that it makes no assumptions about the shape of the droplet size distribution. In contrast, the other vertical weighted droplet size, $r_{e,W}$, implicitly assumes that all of the variability in the vertical profile of droplet size distribution properties is attributable to r_e.

In addition to being influenced by vertical weighting, the bispectral retrieval also makes assumptions about the shape of the droplet size distribution. It is assumed to take the form of a gamma distribution described by two shape parameters, r_e, and the effective variance, v_e (a third parameter simply scales the distribution). While r_e is related to the modal radius, v_e is related to the width of the distribution. Unfortunately, due to limited information content spectral reflectances are less sensitive to changes in v_e, and thus, the bispectral approach is forced to assume a fixed value for v_e (i.e., $v_e = .1$ in the operational MODIS cloud property retrieval). In order to isolate vertical profile effects from the influence of these microphysical assumptions the r_e (3.7 μm) retrieval will be substituted with the vertically weighted r_e(2WT) retrieval proxy. Further discussion of the differences between r_e(2WT) and the bispectral r_e retrieval is provided in the discussion section.

3. Model and Methodology

The main tool employed in this study is a satellite retrieval simulator in combination with an LES model (DHARMA) with bin microphysics [*Ackerman et al*., 2004; *Zhang et al*., 2012]. The LES provides 3-D cloud fields with freely evolving cloud microphysical profiles, which are used as ground truth when comparing with numerically simulated retrievals based on those same fields. The simulator serves as our test bed for exploring hypotheses, helping us overcome the first challenge mentioned in the previous section. The analysis is as follows: We start with radiative transfer simulations based on the output cloud fields from the LES. Subsequently, the bispectral retrieval algorithm is performed on the simulated radiances to obtain the simulated τ, r_e, and LWP retrievals. To make sense of the simulated retrievals, a vertical weighting analysis is performed using the analytical vertical weighting functions in equations 9–14 to obtain r_e(2WT). Finally, the simulated retrievals are compared with the theoretical expectations based on r_e(2WT) and the LES scene properties to investigate the impact of cloud vertical profile on the LWP retrievals.

The LES here adopts 25 size bins to represent droplet size distributions [*Ackerman et al*., 1995]. Unlike a parameterized cloud microphysics scheme, this method makes no assumptions about the shape or number of modes of the droplet size distribution. A bin scheme uses basic physical relationships to describe droplet activation, condensation, collision-coalescence, and sedimentation. Conveniently, the bin scheme also allows us to discriminate drizzle drops from cloud droplets by using a bin size cutoff of about 30 μm. Distinguishing these two populations of droplets allows us to examine the impact of the larger drops on remote sensing retrievals. The optical properties of each size bin are computed by bulk averaging Mie scattering properties over a highly resolved flat subbin droplet size distribution.

Radiative transfer calculations are performed using the discrete ordinates radiative transfer model [*Stamnes et al*., 1988], producing 1-D bispectral radiances at the horizontal resolution of the LES grid (described below). The sole consideration of high-resolution 1-D retrievals allows us to isolate the impact of vertical profile effects from other known retrieval biases that exist due to inhomogeneous horizontal structure, and 3-D radiative effects. It should be noted that the background aerosols that serve as cloud condensation nucleus in the model are not included in the radiative transfer scene. All radiative transfer modeling in this work is performed for a single-observation geometry (solar zenith angle, $\theta_0 = 20°$; viewing zenith angle, $\theta_v = 0°$; and relative azimuthal angle, $\Delta\Phi = 30°$).

Three LES cases are analyzed throughout this study. The first (referred to as "ATEX clean" hereafter) and second ("ATEX polluted") cases are based on an idealized case study [*Stevens et al*., 2001] from the Atlantic Trade Wind Experiment (ATEX), with different aerosol loadings. The ATEX cases are considered to be representative of a trade wind cumulus regime in which scattered cumulus rise into a thin, broken stratocumulus layer. For these ATEX simulations [*Fridlind and Ackerman*, 2011] a domain size of $9.6 \times 9.6 \times 3$ km is used, with a uniform horizontal grid of $\Delta x = \Delta y = 100$ m and a fixed vertical grid spacing of $\Delta z = 40$ m. Further details of the model setup for the ATEX cases are provided by *Zhang et al*. [2012]. The third case (referred to as "DYCOMS-II" hereafter) is an idealized setup [*Stevens et al*., 2005] based on clouds observed during the second research flight (RF02) of the Second Dynamics and Chemistry of Marine Stratocumulus project

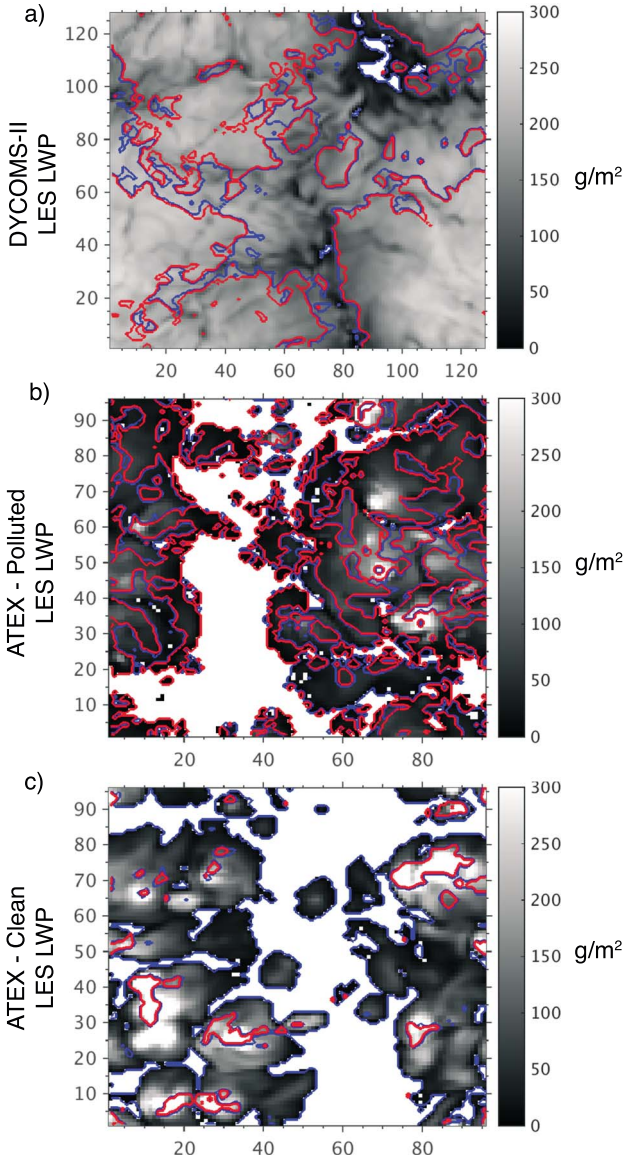

Figure 1. These figures depict the VNIR-SWIR retrieval of cloud LWP with adiabatic assumptions as in equation (3) and using the $r_e(3.7\ \mu m)$ retrieval to represent the cloud top droplet size for several LES cases. The red and blue contours outline regions where the adiabatic (red) or constant (blue) vertical profile assumptions more accurately predicted the LES LWP.

(DYCOMS-II) [*Stevens et al.*, 2003]. This case is considered to be representative of nocturnal marine stratocumulus under a dry inversion. The DYCOMS-II case has a domain size of $6.4 \times 6.4 \times 1.5$ km, with a horizontal grid spacing of $\Delta x = \Delta y = 50$ m and a stretched vertical grid with a minimum spacing of 5 m near the surface and temperature inversion, designed to better resolve small-scale turbulence. Further details of the model setup for the DYCOMS-II case are provided by *Ackerman et al.* [2009]. For each LES case, a snapshot of cloud microphysical properties is saved every half hour over the last 4 h of each simulation, resulting in eight 3-D cloud scenes.

4. Results and Analysis

4.1. LWP Retrievals

With two vertical profile assumptions for LWP retrieval it is natural to ask the question: does the homogeneous $\mathrm{LWP}_h = \frac{2}{3}\rho_l r_e \tau$ or adiabatic $\mathrm{LWP}_{\mathrm{ad}} = \frac{2}{3}\rho_l r_e^{\mathrm{top}} \tau$ relationship compare more closely with the LES ground truth? In an attempt to address this question, Figure 1 provides grayscale images showing $\mathrm{LWP}_{\mathrm{LES}}$ for the three LES cases. The biases of LWP_h and $\mathrm{LWP}_{\mathrm{ad}}$ relative to $\mathrm{LWP}_{\mathrm{LES}}$ are then used to identify which retrieval is "favored". The favored retrieval assumption is simply the one with a smaller absolute bias. The red contour lines in Figure 1 surround retrieval pixels that favor adiabatic vertical profile assumptions, while the blue contour lines surround retrieval pixels that favor homogeneous profile assumptions. For this comparison, both of the retrievals make use of the MODIS-like bispectral $r_e(3.7\ \mu m)$ and τ_{tot} retrievals. To address LES columns that do not overwhelmingly favor either retrieval, a third population is defined, and these columns lie in the space between the red and blue contour lines. This population is defined by the following tolerance condition on the ratio of the two biases,

$$0.75 \leq \frac{|\mathrm{LWP}_h - \mathrm{LWP}_{\mathrm{LES}}|}{|\mathrm{LWP}_{\mathrm{ad}} - \mathrm{LWP}_{\mathrm{LES}}|} \leq 1.25. \quad (15)$$

The lower and upper ends of the inequality correspond to cases that favor homogeneous and adiabatic assumptions, respectively. It is intriguing to observe that none of the three cases support a single retrieval assumption but rather indicate that $\mathrm{LWP}_{\mathrm{ad}}$ works better for some columns, while LWP_h works better for others. As summarized in the first column of Table 1, the $\mathrm{LWP}_{\mathrm{ad}}$ retrieval works better for about 70% of the

Table 1. Percentage of Columns That Favor Adiabatic, Homogeneous, or Neither LWP Retrieval[a]

		Steps of Procedure								
		1. Original Scene			2. Remove Drizzle			3. Remove Drizzle and Transition Zone		
Favored Profile Assumption		5/9	2/3	Neither	5/9	2/3	Neither	5/9	2/3	Neither
LES Case	DYCOMS-II	70.7%	19.1%	10.2%	91.5%	4.0%	4.5%	96.3%	1.5%	2.2%
	ATEX clean	21.7%	73.2%	5.1%	41.5%	49.8%	8.7%	54.2%	37.3%	8.5%
	ATEX polluted	69.8%	19.3%	10.9%	69.8%	19.3%	10.9%	84.4%	3.6%	12%

[a]The rows separate different LES cases and the columns distinguish the removal of features. The statistics are aggregated over all scenes for each case.

cloudy LES columns in the DYCOMS-II case, 22% in the ATEX clean case, and 70% in the ATEX polluted case. The most appropriate retrieval assumption appears to depend on cloud regime.

4.2. LWP Retrieval Bias Budget

Biases in the bispectral LWP retrieval can result from a number of sources. The retrieval is sensitive to biases resulting from the a priori vertical profile assumption as well as the biases in the τ and r_e retrievals that LWP is calculated from. To identify the importance of the bias resulting from cloud vertical profile assumptions, we consider the total bias budget of the LWP retrieval. Treating each of the biases as a deviation away from the actual LES properties leads to the following bias budget:

$$\begin{aligned} \mathrm{LWP}_{\mathrm{ret}} &= \mathrm{LWP}_{\mathrm{LES}} + \Delta\mathrm{LWP} \\ &= (C_{\mathrm{LES}} + \Delta C)\rho_l\left(r_{e,\,\mathrm{LES}} + \Delta r_e\right)(\tau_{\mathrm{LES}} + \Delta\tau), \end{aligned} \tag{16}$$

from which the first-order terms can be extracted:

$$\Delta\mathrm{LWP}_C \approx (C_{\mathrm{ret}} - C_{\mathrm{LES}})\rho_l r_{e,\,\mathrm{LES}}\tau_{\mathrm{LES}}, \tag{17}$$

$$\Delta\mathrm{LWP}_{r_e} \approx C_{\mathrm{LES}}\rho_l\left(r_{e,\,\mathrm{ret}} - r_{e,\,\mathrm{LES}}\right)\tau_{\mathrm{LES}}, \tag{18}$$

$$\Delta\mathrm{LWP}_{\tau} \approx C_{\mathrm{LES}}\rho_l r_{e,\,\mathrm{LES}}(\tau_{\mathrm{ret}} - \tau_{\mathrm{LES}}). \tag{19}$$

where the subscript ret denotes retrieved properties and the subscript LES denotes properties taken from the LES scene itself. These biases are reported in units of g/m^2 and are referred to here as the vertical profile assumption bias $\Delta(\mathrm{LWP}_C)$, the r_e retrieval bias $(\Delta\mathrm{LWP}_{r_e})$, and the τ retrieval bias $(\Delta\mathrm{LWP}_{\tau})$. Although not shown here, higher-order cross terms obtained by fully factoring equation (16) account for a very small portion of the overall LWP retrieval bias, so we neglect them throughout. The value of τ_{LES} can be obtained from LES microphysics in a straightforward manner, while the definition of $r_{e,\mathrm{LES}}$ and C_{LES} require further introduction. The definition of $r_{e,\mathrm{LES}}$ is tied to the definition of cloud top, which we define operationally for each LES column with respect to the cloud maximum LWC located near the optical cloud top (defined as the first cloudy element with $\tau > 10^{-3}$),

$$r_{e,\,\mathrm{LES}} \equiv r_e^* = r_e(z(\max[\mathrm{LWC}])). \tag{20}$$

with $r_{e,\mathrm{LES}}$ recast as r_e^* to recognize that its value depends on the definition of cloud top. The definition of cloud top will be further discussed in the proceeding section. The definition of C_{LES} depends on the coupled relationship between other LES properties outlined in equation (1),

$$C_{\mathrm{LES}} = \frac{\mathrm{LWP}_{\mathrm{LES}}}{r_{e,\,\mathrm{LES}}\tau_{\mathrm{LES}}}. \tag{21}$$

The bias budget presented here allows for the evaluation of the relative importance of each of the primary biases. Analysis of both the spatial distribution and histograms of these primary bias terms yields interesting insight. The spatial distributions of each of the terms in the bias budget for the DYCOMS-II $\mathrm{LWP}_{\mathrm{ad}}$ retrieval ($C_{\mathrm{ret}} \equiv 5/9$) are shown in Figures 2a–2c. These results reveal that the profile assumption bias and the r_e retrieval bias are nonuniformly distributed, in contrast with the more uniformly distributed τ retrieval bias. Moreover, the profile assumption bias and the r_e retrieval bias appear to be spatially correlated with the contours defining the retrieval-favoring populations in Figure 1a. Histograms of these biases, seen in Figures 2d–2f, reveal that the magnitude of the vertical profile assumption bias is also highly varied, with some of the population biased high and some low. In contrast, the distributions of the r_e and τ retrieval biases are substantially narrower and on average smaller than the vertical profile bias. Motivated by this case, the focus of the remainder

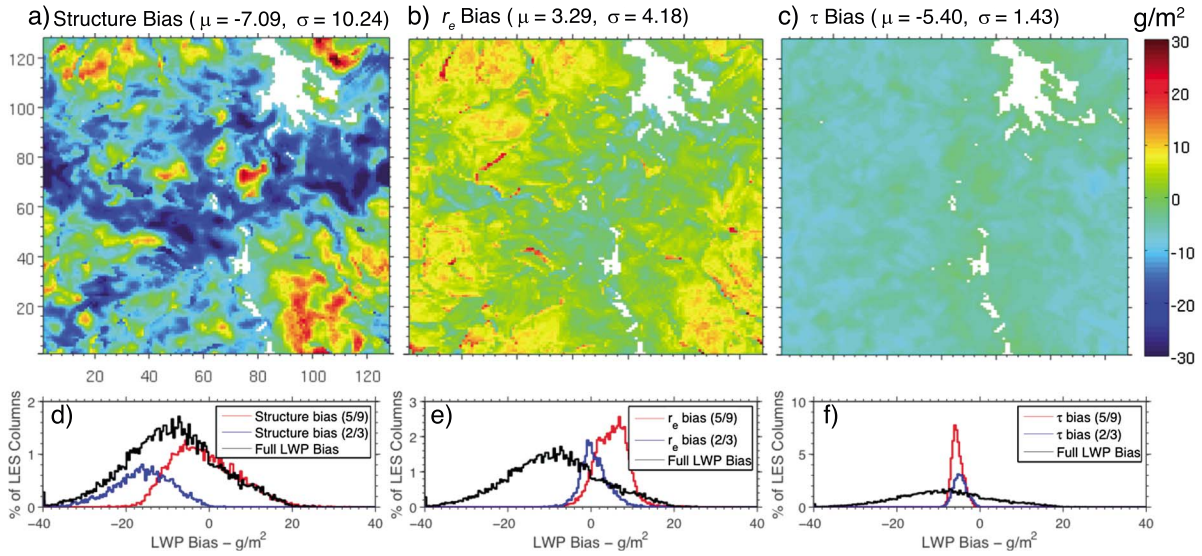

Figure 2. The LWP bias budget for a DYCOMS-II scene is broken into (a, c) the profile bias, (b, d) the r_e bias, and (c, e) the τ bias. Figures 2a–2c depict the spatial distributions of these biases, while Figures 2d–2f depict their corresponding histograms. The mean and standard deviation (μ and σ) of each of the biases in this scene are stated above Figures 2a–2c in units of g/m^2. Together these results demonstrate that the profile assumption bias dominates the LWP bias budget (see text).

of this study will be on the impact of cloud vertical profile assumptions and the physical causes of r_e retrieval bias. While only shown for one scene from one LES case, the vertical profile and r_e retrieval biases were each consistently the greatest contributors to the bias budget across all scenes and cases. The τ bias is less deserving of further scrutiny because it cannot account for either the spatial variability or much of the magnitude of the full LWP bias.

4.3. Vertical Profiles of LES Properties

To further understand the impact of cloud vertical profiles on LWP retrievals, the profiles of several cloud properties were discriminated into two retrieval populations (i.e., LWP$_h$ favored versus LWP$_{ad}$ favored). The median vertical profiles for the DYCOMS-II case in Figures 3a and 3b demonstrate that both LWP$_h$-favored (blue) and LWP$_{ad}$-favored (red) columns have similar vertical profiles in terms of CDNC and LWC. The profile of CDNC remains relatively constant within the cloud, with the LWP$_h$-favored columns having on average a smaller CDNC than those LWP$_{ad}$-favored columns. The LWC profiles for both populations show a characteristic linear increase with height associated with the subadiabatic assumption. However, the most distinguishing feature of the two populations appears to be the vertical profile of r_e. Clearly, the LWP$_{ad}$-favored columns have simpler vertical profiles within the cloud layer, with r_e monotonically increasing from cloud base upward, unlike the LWP$_h$-favored columns, which have a more complex vertical profile of r_e. Below cloud base r_e is seen to increase rapidly downward for both populations. This signature is indicative of the predominant impact that growth from collisional-coalescence and vertical size sorting can have on the r_e profile at those levels.

Shifting from a physical profile perspective to an optical profile perspective, Figure 4 depicts the vertical profile of LWC and r_e as a function of cloud optical depth. Given that scattering exponentially attenuates reflected light as a function of τ, it is appropriate to plot optical profiles logarithmically with respect to τ. What is evident from these optical profiles is that there is a region above cloud top (defined by the maximum LWC and indicated by the horizontal dashed line) where r_e is modestly reduced from its value at cloud top $\left(r_e^*\right)$. In this region LWC also transitions from its maximum at cloud top to its cloud-free value of zero as dry air from above cloud top becomes entrained and mixed with the upper region of the cloud. This reduction in LWC is indicative of inhomogeneous mixing or, more simply, dilution, in which mixing resolved by the model is faster than evaporation [*Baker and Latham*, 1979]. However, the modest reduction of r_e in this region also serves as an indicator that some evaporation is also occurring. Hereafter, we shall refer to this region as the cloud top transition zone. The peak LWC is used to define the base of the transition zone, which then

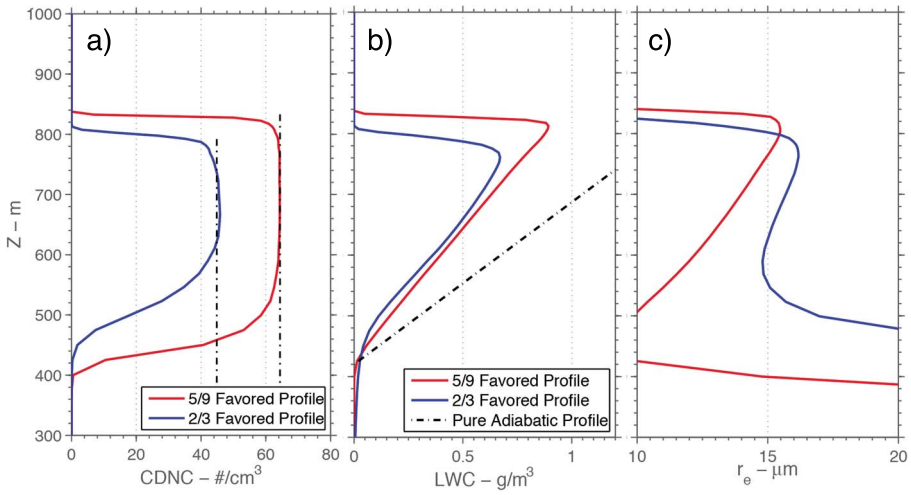

Figure 3. Median profiles of (a) CDNC, (b) LWC, and (c) r_e for the DYCOMS-II scene from Figure 2 when divided into two LWP retrieval bias populations (see Figure 1). The blue lines correspond to columns favoring the homogeneous vertical assumption ($C = 2/3$), and the red lines correspond to the adiabatic vertical assumption ($C = 5/9$). The dash-dotted lines in Figures 3a and 3b depict the constant CDNC assumption and the adiabatic LWC profile, respectively.

extends upwards toward the optical cloud top ($\tau = 10^{-3}$). These artificial boundaries are intended to delimit the region influenced by cloud top entrainment. While the transition zone appears shallow in terms of physical thickness (Figure 3), the optical profile (Figure 4) reveals that the transition zone has a typical optical depth of 1–2. This is important because, as mentioned in section 2, absorption in the SWIR band leads to a retrieval exponentially weighted toward the uppermost region of the cloud. It follows that a transition zone of this thickness could impact the retrieved droplet size, and thus, it can indirectly influence LWP retrievals. However, the behavior of the transition zone does not appear to significantly differentiate the two retrieval-favoring populations. Looking toward the cloud base in Figure 4b, it is clear that the two populations differ significantly. As Figure 4c reveals, this difference is absent after removing drizzle. In fact, the removal of drizzle leaves both profiles resembling one another, in addition to matching well with the form of the theoretical adiabatic profile (the black dash-dotted curve in Figure 4c).

4.4. Impact of Drizzle and the Cloud Top Transition Zone

As discussed above, the cloud vertical profiles observed in these LES cases differ from adiabatic profiles mainly due the presence of drizzle and a cloud top transition zone. The impacts of these features on the LWP retrievals are explained using the hypothetical profiles of r_e shown in Figure 5. To make the explanation easier, we first define two reference effective radii, $r_e(5/9)$ and $r_e(2/3)$, by rearranging equation (1) and substituting the appropriate constant as well as the LWP and τ_{tot} from the LES:

$$r_e(5/9) = \frac{9}{5}\frac{\mathrm{LWP_{LES}}}{\rho_l \tau_{\mathrm{tot,\ LES}}}, \tag{22}$$

$$r_e(2/3) = \frac{3}{2}\frac{\mathrm{LWP_{LES}}}{\rho_l \tau_{\mathrm{tot,\ LES}}}. \tag{23}$$

These are the droplet sizes that are required to complete the assumed relationship between LWP, r_e, and τ_{tot} for either of the vertical profile assumptions. These droplet sizes serve as litmus tests: If the in situ cloud top droplet effective radius, r_e^*, better matches with $r_e(5/9)$ than with $r_e(2/3)$, then the LES column favors $\mathrm{LWP_{ad}}$ vertical profile assumptions and where closer to $r_e(2/3)$ it favors LWP_h vertical assumptions. The ideal adiabatic profile in Figure 5a demonstrates that r_e^* and $r_e(5/9)$ would perfectly match when the actual profile is adiabatic. This stands in contrast with $r_e(2/3)$, which is smaller because the LWP_h profile assumption overestimates the actual LWP. In addition to the vertical profile assumed in the LWP calculation, there is also the impact of vertical weighting on the underlying droplet size retrieval. For the adiabatic profile in Figure 5a, $r_{e,\mathrm{2WT}}$ matches r_e^* very well, indicating that the vertically weighted droplet size would provide a reasonable

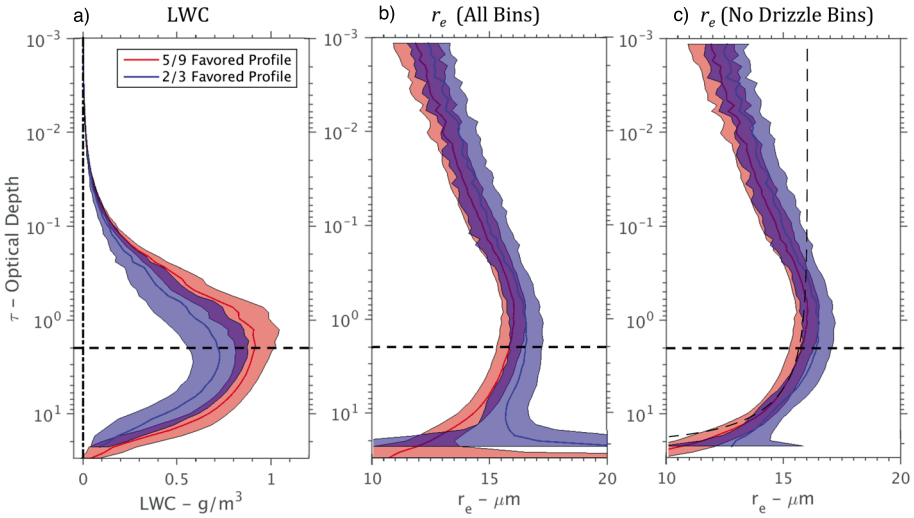

Figure 4. Optically binned profiles of (a) LWC, (b) r_e with drizzle bins included, and (c) r_e without contribution of drizzle bins from the DYCOMS-II case. The optical depths refer to the 3.75 μm band. As discussed in the text, drizzle is defined as drops larger than 30 μm. The lines denote median profiles of the columns that favor LWP_{ad} (red) and LWP_h assumptions (blue), while the enveloping contours around the curves denote the interquartile range (IQR) envelope centered about the median. In Figure 4b the large IQR of the last two bins of the 2/3 favored profile fall well outside of the plotting range with values IQR = [16, 30.7].

estimate of the cloud top droplet size for such a cloud. The comparisons of $r_e(5/9)$ and $r_{e,2WT}$ to r_e^* indicate, as expected, that the adiabatic retrieval provides an accurate representation of LWP_{LES} for an adiabatic cloud. A second hypothetical case seen in Figure 5b adds complexity by including drizzle near cloud base to mimic the cloud profiles from the LES as seen in Figures 3 and 4. In this case the retrieval proxy $r_{e,2WT}$ is still a good match to cloud top r_e^* because the SWIR band reflectance saturates near cloud top and is largely insensitive to the presence of drizzle lower in the cloud. However, as demonstrated in the schematic, the presence of drizzle can cause both $r_e(5/9)$ and $r_e(2/3)$ to be larger than r_e^* in proportion to the amount of LWP in the drizzle mode. This bias reflects the increase in the ratio of LWP_{LES} to $\tau_{tot,LES}$ in equations (22) and (23). This shift in

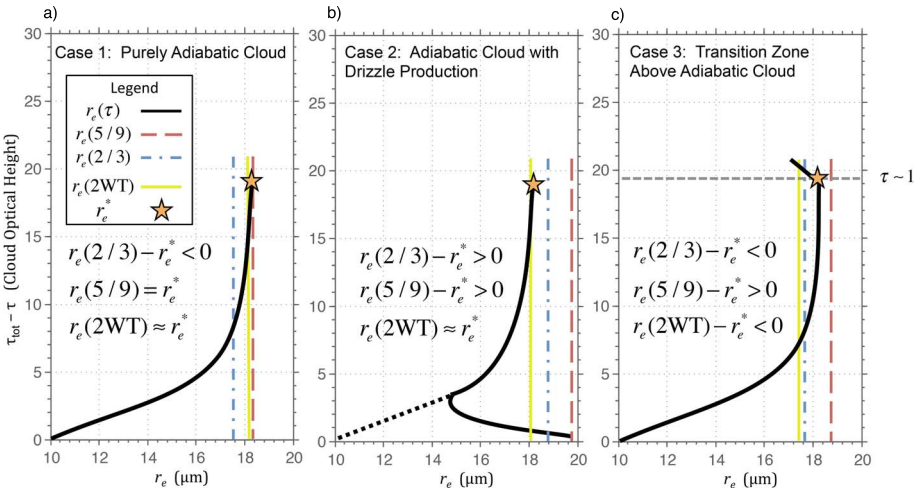

Figure 5. Several common cloud vertical profile cases in the LES. These optical profiles are defined in terms of cloud optical height to maintain consistency between the characteristic equation describing an adiabatic vertical profile. The vertical blue and red dash-dotted lines represent the value of the vertical profile assumption-required droplet sizes $r_e(2/3)$ and $r_e(5/9)$ respectively. The yellow line represents the value of the optical retrieval $r_e(2WT)$ and the gray dashed line in Figure 5c represents the location of the base of the transition zone. The yellow star represents both the location and value of the cloud top droplet size r_e^*.

the ratio occurs because LWP_{LES} is sensitive to the increase in the $r_e(\tau)$ profile lower in the cloud, as indicated in the integral in equation (5). It follows that a high bias of $r_e(2/3)$ indicates that, compared to LWP_{LES}, the LWP_h retrieval would be biased low and the LWP_{ad} lower yet. With that in mind, a positive $r_e(2/3) - r_e^*$ bias can serve as an indicator of the influence of drizzle on vertical profile. A third hypothetical case, shown in Figure 5c, addresses the impact of the cloud top transition zone. In this zone, r_e decreases modestly with height (increases with optical depth for $\tau < 2$) from the value at cloud top, r_e^*. The optical thickness of this transition zone is large enough to influence the vertically weighted retrieval, $r_{e,2WT}$, which would be low biased relative to r_e^*. A low bias in the cloud top r_e retrieval would subsequently lead to a low bias in both LWP calculations. In contrast, to the extent that the transition zone is optically thin, $r_{e,2WT}$ would serve as an accurate description of the cloud top droplet size.

Considering the impacts of the cloud top transition zone and drizzle we now ask, what happens to LWP retrieval biases when these two features are removed from an LES cloud scene? If it were correct to treat these features as the primary drivers of nonadiabatic cloud profiles, then we would expect adiabatic retrieval assumptions to better match the actual LWP upon the removal of these features. To organize these comparisons, we introduce two r_e biases: (1) a *profile bias*, which compares the vertical profile retrieval assumptions with LES profiles, and (2) a *retrieval bias*, which compares the vertically weighted 2WT retrieval proxy to LES profiles:

$$r_e \text{ profile bias} \equiv r_e(5/9) - r_e^* \tag{24}$$

$$r_e \text{ retrieval bias} \equiv r_e(2\text{WT}) - r_e^*. \tag{25}$$

These two biases are used to identify features of the schematics in Figure 5 and allow for the intercomparison of retrieval uncertainty associated with droplet size retrievals (retrieval bias) and profile assumptions in LWP retrievals (profile bias). This method is convenient because it decouples sensitivity to drizzle and the transition zone. The profile bias is primarily sensitive to the presence of drizzle because of its influence on $r_e(5/9)$ due to the changing vertical profile of $r_e(\tau)$ (refer to Figure 5b), whereas the retrieval bias is primarily sensitive to the impact of the transition zone at the cloud top because of the vertically weighted droplet size retrieval (refer to Figure 5c). Each bias is compared relative to the droplet size at the peak LWC, r_e^*, as a point of reference.

With the retrieval and profile biases as diagnostics we can now examine what happens to the quality of LWP retrievals as these two features are removed from an LES scene. The removal of drizzle involves simply removing droplets in size bins larger than the 30 μm cutoff from all LES quantities and subsequent retrievals, while the transition zone removal is accomplished by excluding this region at the top of the cloud from the LES LWP and optical thickness as well as the r_e(2WT) retrieval proxy. This removal experiment is performed sequentially, with drizzle removed first, followed by the transition zone. It should be noted that the order of the sequence was determined to be unimportant because the biases from drizzle and the transition zone are sufficiently decoupled. As depicted in Figure 6, the joint analysis of the profile and retrieval biases demonstrates how sequential removal of drizzle and the transition zone influence LWP retrievals. For example, the impact of drizzle can be understood by looking at the points around upper horizontal dashed line, which denotes the location of zero bias for $r_e(2/3) - r_e^*$ on the $r_e(5/9) - r_e^*$ axis. As mentioned previously, drizzle can induce a positive bias in r_e(2/3) and an even greater bias in r_e(5/9) (refer to Figure 5b). Removal of drizzle removes nearly all occurrences of positive $r_e(2/3) - r_e^*$, as evidenced by the change in bias between the scatterplots in Figures 6a and 6b. In the final removal step, after the transition zone is removed in Figure 6c, there is a drastic improvement in the retrieval bias resulting in almost no dispersion and only a slight negative bias. The removal of drizzle and entrainment zone features causes the DYCOMS-II case to go from nearly a 50-50 split regarding favored vertical profile assumption to more than 95% in favor of the adiabatic vertical profile assumption. The fraction of the DYCOMS-II columns favoring adiabatic, homogeneous, or neither retrieval assumption is shown in the first row of Table 1 for each of the removal experiment steps. It is worth noting that the remaining columns that favor homogeneous vertical assumptions appear to be located near cloud holes where entrainment of dry air can occur through the side of the cloud. It thus appears plausible that the transition zone at horizontal cloud boundaries can contribute to LWP retrieval bias as well.

As already mentioned, previous studies have indicated that bispectral LWP retrieval bias is dependent on cloud regime. Thus far, we have highlighted a single LES case (DYCOMS-II) and snapshot, but an examination of the other LES cases offers the opportunity to study how another MBL cloud regime is influenced by vertical

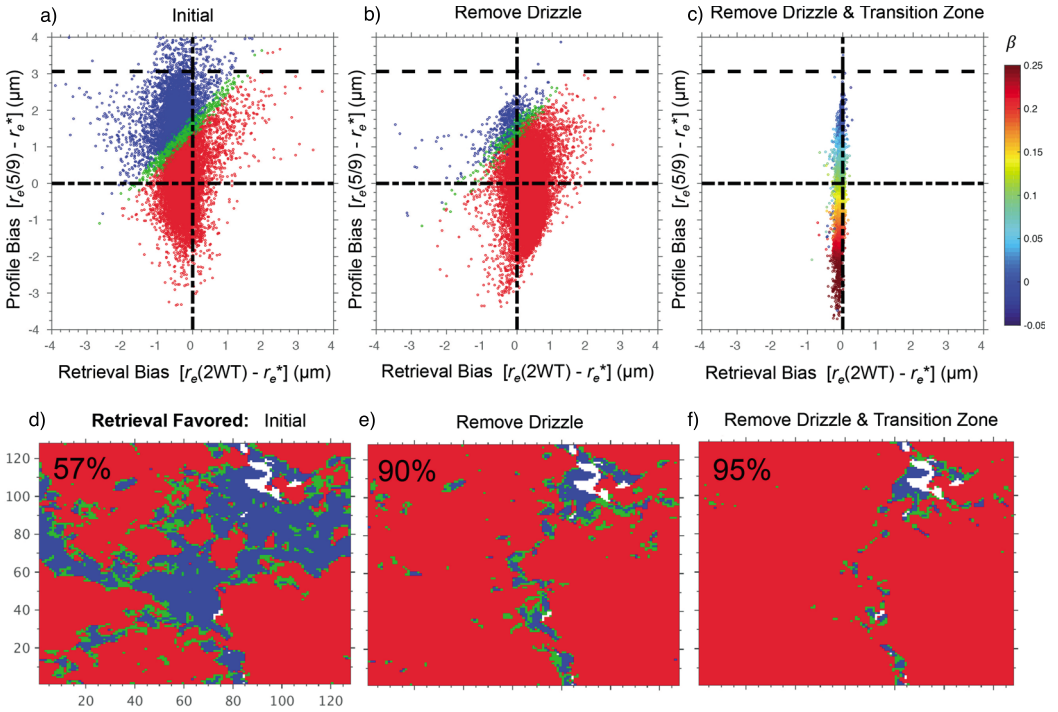

Figure 6. The sequential removal analysis for the DYCOMS-II LES scene introduced in Figure 1. (a–c) The impact of the removal of drizzle and then transition zone on the profile and retrieval biases. The dash-dotted lines in Figures 6a–6c denote neutral bias, whereas the horizontal dashed line denotes the value of r_e(5/9) profile bias that corresponds to neutral r_e(2/3) profile bias. The colors in scatterplots (Figures 6a and 6b) are associated with the (d and e) retrieval quality maps, where red denotes LWP retrievals favoring LWP_{ad}, blue with LWP_h, and green with neither. Note that the retrieval quality map in Figure 6d corresponds to the contours in Figure 1a. The inset percentages indicate the share of pixels that favor LWP_{ad}. The color of points in Figure 6c depicts the droplet optical growth exponent, β (see text), after (f) drizzle and the transition zone features have been omitted.

profile assumptions. A comprehensive view of the model cases and time slices requires a statistical approach. The mean bias for a case represents the systematic bias from vertical profile and retrieval assumptions, and the standard deviation of the bias is associated with the variability within the LES. The results, provided in Table 2, further demonstrate that the relative importance of drizzle and the transition zone are associated with cloud regime. These results are also informed by the cloud fraction and LWP information in Table 3. For the DYCOMS-II case, the overall reduction of mean and standard deviation of biases indicates that the removal of both features leads toward increasing agreement with adiabatic retrieval assumptions. The statistical results from the ATEX cases do not exhibit the same behavior. As we saw before, the ATEX clean case strongly favors homogeneous retrievals at the outset. The contribution of drizzle to LWP in this case is appreciable (see Table 3), and as a consequence, the removal of drizzle leads to a reduced mean and standard deviation of profile biases. The ATEX clean case does not converge toward adiabatic assumptions by the final removal step and the remaining regions that do not favor adiabatic assumptions are narrow, lie in the vicinity of cloud edge, and surround thick convective cores that favor adiabatic assumptions (not shown). As mentioned previously, horizontal cloud boundaries near cloud holes are potentially influenced by entrainment horizontally as well as from cloud top. The low cloud fraction in this case (see Table 3) increases the prevalence of horizontal cloud boundaries making it difficult to distinguish the influence of entrainment and drizzle in these regions. For the ATEX clean case homogeneous assumptions yield less bias than the adiabatic assumptions when drizzle is prominent. However, in the ATEX polluted case, which lacks drizzle (see Table 3), the retrievals are little affected by omitting it. The retrieval assumption favored by the ATEX polluted case is not driven by a systematic (mean) bias, as was the case for the DYCOMS-II and ATEX clean cases. Instead, the rather large variability (standard deviations) in both biases leads to instances where either of the LWP retrieval assumptions satisfy portions of the population. Upon removal of the entrainment features the ATEX polluted case clearly favors adiabatic retrievals, as indicated in Table 1. However, as with the ATEX clean case, the majority of columns that do not favor adiabatic retrievals are again found near horizontal cloud boundaries

Table 2. Aggregated Statistics for the Profile Bias and Retrieval Bias of r_e[a]

	r_e Bias Statistics (μm)					
	Profile Bias [$r_e(5/9) - r_e^*$]			Retrieval Bias [$r_e(2WT) - r_e^*$]		
LES Case	Original Scene	Removal of Drizzle	Removal of Drizzle and Transition Zone	Original Scene	Removal of Drizzle	Removal of Drizzle and Transition Zone
DYCOMS-II	$\mu = 0.55$ ($\sigma = 1.03$)	$\mu = -0.0704$ ($\sigma = 0.840$)	$\mu = -0.254$ ($\sigma = 0.832$)	$\mu = -0.217$ ($\sigma = 0.401$)	$\mu = -0.232$ ($\sigma = 0.409$)	$\mu = -0.0696$ ($\sigma = 0.0597$)
ATEX clean	$\mu = 2.84$ ($\sigma = 2.51$)	$\mu = 1.38$ ($\sigma = 1.37$)	$\mu = 1.30$ ($\sigma = 1.65$)	$\mu = 0.393$ ($\sigma = 1.96$)	$\mu = -0.324$ ($\sigma = 1.21$)	$\mu = -0.016$ ($\sigma = 0.311$)
ATEX polluted	$\mu = 0.122$ ($\sigma = 0.586$)	$\mu = 0.124$ ($\sigma = 0.585$)	$\mu = 0.084$ ($\sigma = 0.610$)	$\mu = -0.107$ ($\sigma = 0.681$)	$\mu = -0.108$ ($\sigma = 0.681$)	$\mu = -0.0066$ ($\sigma = 0.0752$)

[a]Rows are as in Table 1, while columns are broken into sections for profile and retrieval biases, which are then broken down into subsections by removal step. The mean and standard deviation are given by μ and σ.

(not shown). To summarize some of the foregoing discussion, major distinctions between the ATEX clean and polluted cases can be drawn. The first is that while drizzle plays a dominant role in the clean case, it is negligible in the polluted case. The second is that the polluted case has significantly fewer columns associated with cloud horizontal boundaries and favors adiabatic retrievals more on the whole after removal of entrainment features. The varied difference in these findings across just these three cases demonstrates that bispectral LWP retrieval biases depend on cloud regime as well as the presence of drizzle. Furthermore, the differences highlight the fact that there is no single vertical profile assumption suitable for all of these cloud regimes.

The evaluation of retrieval and profile bias statistics in terms of r_e is useful for identifying and comparing the physical causes of LWP retrieval bias, but it does not directly relate these biases to the magnitude of the associated LWP bias. To address this, we also define LWP profile and retrieval biases, which couples r_e variability and τ variability. The LWP profile and retrieval biases are defined as follows:

$$\text{LWP profile bias} \equiv \frac{5}{9}\rho_l r_e^* \tau_{\text{LES}} - \text{LWP}_{\text{LES}} \tag{26}$$

$$\text{LWP retrieval bias} \equiv \frac{5}{9}\rho_l r_e(2\text{WT})\tau_{\text{LES}} - \text{LWP}_{\text{LES}}. \tag{27}$$

The LWP profile and retrieval biases, shown in Table 4, help to put the previous analysis in the context of retrieval outcomes and furthers our arguments about the impact of profile on cloud retrievals. In the presence of drizzle, the LWP profile bias is negative, while the presence of an optically thick transition zone can cause the LWP retrieval bias to be negative as a secondary effect of low-biasing cloud top droplet size retrievals (refer to $r_e(2WT)$ in Figure 5c). Removal of both of these features leads to LWP_{ad} retrievals that are biased low relative to actual LWP. Mean LWP biases are seen in Table 4 to range from values as large as -10 g/m^2 before the features are removed, to values on the order of 1 g/m^2 after removal. Thus, adiabatic assumptions in cloud retrievals can lead to LWP biases on the order of 10–20% in the presence of drizzle and the cloud top transition zone. As with the r_e biases, the mean LWP profile and retrieval biases show improvement as well as a reduction in their standard deviation as the features are removed. The remaining variability in these biases and their dependence on cloud regime are likely attributable to unaccounted behavior in the passive LWP retrieval technique, i.e., the assumption that the droplet number concentration is constant throughout the cloud, which we consider next.

Table 3. Aggregated Statistics for Each of the LES Cases Cloud Fraction, Median LWP and Percent of LWP-Associated Drizzle[a]

LES Case	Cloud Fraction	Median LWP (g/m^2)	%LWP (Drizzle)
DYCOMS-II	99.4%	163.6	4.0%
ATEX clean	34.8%	71.5	13.0%
ATEX polluted	40.2%	35.6	<0.1%

[a]All properties are listed for the initial state of the LES scene before the removal experiment.

Table 4. As in Table 2 but for LWP

	LWP Bias Statistics (g/m^2)					
	Profile Bias [LWP(5/9) − LWP_{LES}]			Retrieval Bias [LWP(2WT) − LWP_{LES}]		
LES Case	Original Scene	Removal of Drizzle	Removal of Drizzle and Transition Zone	Original Scene	Removal of Drizzle	Removal of Drizzle and Transition Zone
DYCOMS-II	$\mu = -5.79$ ($\sigma = 8.81$)	$\mu = 2.89$ ($\sigma = 7.70$)	$\mu = 4.41$ ($\sigma = 7.31$)	$\mu = -2.64$ ($\sigma = 3.61$)	$\mu = -2.76$ ($\sigma = 3.64$)	$\mu = -0.990$ ($\sigma = 0.575$)
ATEX clean	$\mu = -9.42$ ($\sigma = 12.4$)	$\mu = -0.834$ ($\sigma = 7.88$)	$\mu = 1.95$ ($\sigma = 8.09$)	$\mu = -3.37$ ($\sigma = 9.15$)	$\mu = -5.76$ ($\sigma = 11.8$)	$\mu = -2.70$ ($\sigma = 3.83$)
ATEX polluted	$\mu = -0.63$ ($\sigma = 4.29$)	$\mu = 0.368$ ($\sigma = 4.71$)	$\mu = 0.878$ ($\sigma = 4.71$)	$\mu = -1.33$ ($\sigma = 7.23$)	$\mu = -1.33$ ($\sigma = 7.40$)	$\mu = -0.0156$ ($\sigma = 0.0712$)

4.5. Vertical Profile Variability

Beyond the impact of drizzle on the r_e profile bias the large variability remaining after removal of drizzle and entrainment features remains unexplained. For the adiabatic retrieval, this variability suggests that there are additional aspects of the simulated clouds that are inconsistent with adiabatic assumptions. In an attempt to explain this variability, we return to the adiabatic profile described in equation (7) and note that the profile of $r_e(\tau)$ can be expressed as a simple power law relationship

$$r_e(\tau) = \alpha\left(\frac{\tau_{\text{tot}} - \tau}{\tau_{\text{tot}}}\right)^{\beta}. \tag{28}$$

Hereafter, we refer to the exponent, β, as the "droplet optical growth exponent," or sometimes "growth exponent" for the sake of brevity. For an adiabatic profile the value of the droplet optical growth exponent is $\beta_{\text{ad}} = {}^{1}/_{5} = 0.2$. Taking the logarithm of both sides of equation (28), solving for β, and taking a derivative yields an expression with fewer unknown constants

$$\beta = \frac{\text{dlog}(r_e)}{\text{dlog}(\tau_{\text{tot}} - \tau)}. \tag{29}$$

If β was constant throughout the cloudy column, then equation (33) results in the droplet growth exponent in equation (30), which now describes β in terms of $r_e(\tau)$, the total optical thickness and cloud top droplet size.

$$\beta = \frac{\log(r_e^*) - \log(r_e)}{\log(\tau_{\text{tot}}) - \log(\tau_{\text{tot}} - \tau)} = \frac{\log(r_e^*/r_e)}{\log(\tau_{\text{tot}} - \tau)} \tag{30}$$

A recasting of equation (28) avoids the constant α,

$$r_e(\tau) = r_e^*\left(\frac{\tau_{\text{tot}} - \tau}{\tau_{\text{tot}}}\right)^{\beta}. \tag{31}$$

This is the same form as equation (7), and as we did before with the adiabatic case in equation (8), we can also derive a more general LWP expression that includes our definition of the droplet growth exponent.

$$\begin{aligned} \text{LWP} &= \frac{2}{3}\rho_l\int_0^{\tau_{\text{tot}}} r_e(\tau)\text{d}\tau \\ &= \frac{2}{3}\rho_l\frac{1}{\beta+1}r_e^*\left(\frac{1}{\tau_{\text{tot}}}\right)^{\beta}(\tau_{\text{tot}})^{\beta+1} \\ &= \frac{2}{3}\rho_l\frac{1}{\beta+1}r_e^*\tau_{\text{tot}} \end{aligned} \tag{32}$$

In practice, we calculate the value of β discretely between each layer of the LES, as expressed in equation (33) in which β depends on the LES vertical grid index i,

$$\beta_i = \frac{\log(r_{e,\,i}) - \log(r_{e,\,i+1})}{\log(\tau_{\text{tot}} - \tau_i) - \log(\tau_{\text{tot}} - \tau_{i+1})}. \tag{33}$$

We then compute a vertically weighted average of β with the weighted sum of each layer by its optical thickness,

$$\beta = \frac{\sum_i^{N-1}\beta_i\Delta\tau_{i,\,i+1}}{\tau_{\text{tot}}}. \tag{34}$$

Now it is clear from equation (32) that values of $\beta = 0$ and $\beta = {}^1/_5 = 0.2$ lead to the respective definitions of LWP for homogeneous and adiabatic vertical profiles that were introduced in equations (2) and (3). As was evident from Figure 6c the value of β associated with zero adiabatic profile bias is somewhat smaller ($\beta \approx 0.13$) than the expected adiabatic value, ($\beta_{ad} \equiv 0.2$). Perhaps the most striking feature in Figure 6c is the broad variability in the droplet optical growth exponent. We speculate that this variability in growth exponent can be associated with the sensitivity to other implicit assumptions in equation (7). Evidently, many of the DYCOMS-II LES profiles have been modified by diabatic processes (i.e., precipitation and radiative heating) leading to violation of two implicit assumptions of the adiabatic model. First, the cloud droplet number concentration is not consistently vertically uniform. Second, the dispersion of the cloud droplet size distribution is also not vertically uniform. To address this, it is important to introduce the complete expression for the adiabatic profile of r_e,

$$r_{e,\,\mathrm{ad}}(\tau) = \left[\frac{5}{3}\frac{1}{Q_e}\left(\frac{4}{3}\pi\rho_l \frac{1}{f\,\Gamma_{\mathrm{LWC}}}\right)\frac{1}{(kN)^2}\frac{\tau_{\mathrm{tot}} - \tau}{\tau_{\mathrm{tot}}}\right]^{1/5}. \tag{35}$$

The adiabatic $r_e(\tau)$ relationship presented here is a result of the relationship between adiabatic LWC(z), $r_e(z)$, and $\tau(z)$ profiles that has been described throughout the literature numerously [*Pontikis and Hicks*, 1993; *Pontikis*, 1996; *Szczodrak et al*., 2001]. A detailed derivation of this relationship can be found appendix A of *Boers et al*. [2006]. Additional constants are introduced in the adiabatic $r_e(\tau)$ profile, like the degree of adiabaticity and adiabatic LWC lapse rate (f and Γ_{LWC}, respectively); a measure of the droplet size distribution dispersion (k) [*Brenguier et al*., 2011]; and N, the CDNC. As mentioned previously, the adiabatic vertical profile assumption hinges on two implicit assumptions: the effective CDNC (kN) is constant and the droplet size retrieval used is similar to the cloud top droplet size, r_e^*. The observed variability in the values of the droplet optical growth parameter, β, can be attributed to the breakdown of these assumptions. If we assume that both $N(\tau)$ and $k(\tau)$ can also be treated as power law relations, we get the following profiles:

$$N(\tau) \equiv N_0\left(\frac{\tau_{\mathrm{tot}} - \tau}{\tau_{\mathrm{tot}}}\right)^{\eta} \tag{36}$$

$$k(\tau) \equiv \left(\frac{r_v(\tau)}{r_e(\tau)}\right)^3 = k_0\left(\frac{\tau_{\mathrm{tot}} - \tau}{\tau_{\mathrm{tot}}}\right)^{\kappa}, \tag{37}$$

where the new exponents η and κ can be determined in the same manner as was outlined for β. Referring back to the adiabatic vertical profile in equation (8), we can reform equation (28) to account for the profiles $N(\tau)$ and $k(\tau)$,

$$\begin{aligned} r_e(\tau) &= \frac{\alpha}{[k(\tau)N(\tau)]^{2\beta}}\left(\frac{\tau_{\mathrm{tot}} - \tau}{\tau_{\mathrm{tot}}}\right)^{\beta} \\ &= \frac{\alpha}{[k_0 N_0]^{2\beta}}\left(\frac{\tau_{\mathrm{tot}} - \tau}{\tau_{\mathrm{tot}}}\right)^{\beta - 2\beta(\eta+\kappa)} \end{aligned} \tag{38}$$

It should be noted that equation (38) becomes equivalent to equation (7) if η and κ are each zero, which of course leads to both k and N being constant. Nonzero η and κ can lead to a new definition for a reduced effective droplet growth exponent,

$$r_e(\tau) = \alpha'\left(\frac{\tau_{\mathrm{tot}} - \tau}{\tau_{\mathrm{tot}}}\right)^{\beta'} \tag{39}$$

$$\beta' = \beta[1 - 2(\eta + \kappa)]. \tag{40}$$

Hereafter, we will refer to the value of β measured from the LES profile as β' in recognition that it represents a modified adiabatic profile. As previously noted, the DYCOMS-II case displayed a reduced droplet growth exponent of $\beta' \approx 0.13$ associated with the minimum adiabatic profile bias in Figure 6c. This clearly contradicts the theoretical adiabatic value of $\beta_{\mathrm{ad}} = {}^1/_5 = 0.2$. If we consider the median values of the two other exponents, $\eta = 0.039$ and $\kappa = 0.048$, respectively, and an initial droplet growth exponent of $\beta = 0.2$ then equation (40) results in a modified growth exponent of $\beta' = 0.165$. This result, while offering an explanation for the low bias in β values for adiabatic assumptions, still does not explain the source of the broad variability the droplet optical growth rate in Figure 6c. To that end, joint histograms of β' in Figure 7 with respect to both η and κ reveal that β' is sensitive to the observed values of η and κ. The relationship between of η and β' in Figure 7a indicates that much of the broad variability in β' can be traced back to the broadly distributed

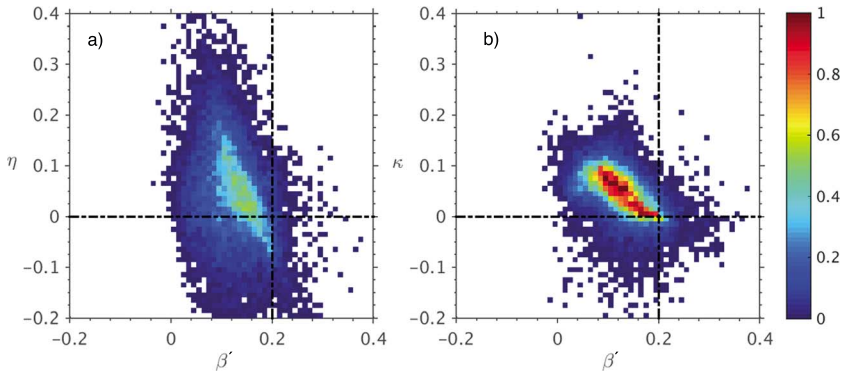

Figure 7. Joint histograms of the droplet growth exponent β' and both of the exponents η and κ introduced in equations (36) and (37), respectively. All quantities are from the LES profiles. The histogram is binned in 0.01 intervals and the color scale is stated in percent. The median values of both η and κ are 0.039 and 0.048 respectively. The dash-dotted lines denote the adiabatic assumptions for each of these exponents.

values of η observed in the LES. While Figure 7b reveals that much of the reduction in the mean value of β' comes from the strong linear dependence of β' on κ.

5. Discussion

Throughout this study several key assumptions are made in order to study the influence of cloud vertical profile on retrievals of cloud LWP: The removal of droplets larger than 30 μm is representative of a cloud without drizzle. The vertically weighted r_e(2WT) is an appropriate proxy for the r_e(3.7 μm) bispectral retrieval. The transition zone appropriately represents the region of the cloud impacted by local entrainment.

The validity of the drizzle assumption was tested directly by turning off collisional-coalescence processes during a DYCOMS-II LES run. The resulting microphysical snapshots revealed that the suppression of droplet growth into drizzle led to a profile bias that was only slightly more reduced than it was by removing "drizzle bins". Thus, it is likely that the impact of drizzle on cloud vertical profile assumptions is slightly greater (on the order of a few g/m^2) than predicted in this study.

The assumption regarding vertical weighting of the 3.7 μm SWIR band can be tested by explicitly using r_e (3.7 μm) in the definition of the retrieval bias (equation (25)) rather than r_e(2WT). The bias scatterplots in Figures 8a–8c correspond to this new definition for the retrieval bias. In contrast to the r_e(2WT) retrieval bias, Figure 8a reveals that, on average, r_e(3.7 μm) has a slight positive bias. A comparison of Figures 6c and 8c also reveals that removal of transition zone features does not dramatically reduce the retrieval bias of r_e(3.7 μm). While it may appear that r_e(2WT) and r_e(3.7 μm) are not perfect analogues, it is important to note the

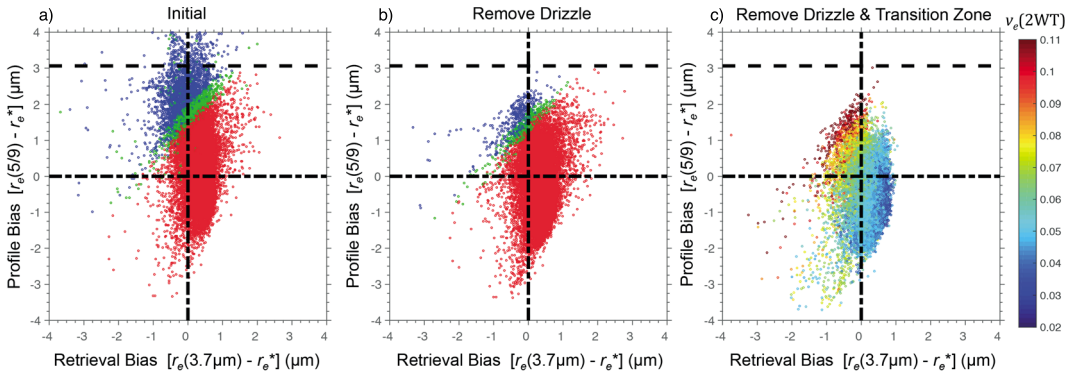

Figure 8. Just as in Figure 6, these profile and retrieval bias scatterplots depict the sequential removal experiment of the DYCOMS-II case snapshot. The difference between the two figures is that the *x* axis depicts the bias of bispectral retrieval r_e (3.7 μm) rather than the vertically weighted r_e(2WT). (a, b) The color of the points is as in Figure 6; (c) the value of the vertically weighted retrieval, v_e(2WT). Refer to Figure 6 for the description of lines and coloration (in Figures 7a and 7b) for these plots.

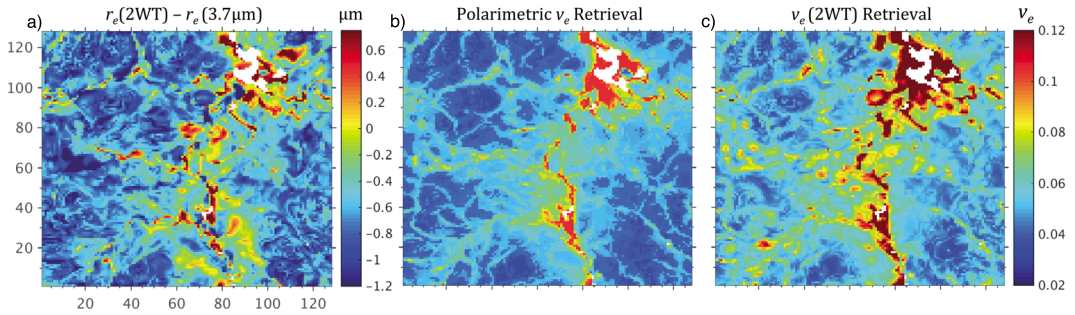

Figure 9. Droplet microphysical retrieval scenes from the DYCOMS-II case. (a) The bias between the 2WT and bispectral r_e retrievals; retrieval of v_e via the (b) polarimetric method and (c) vertically weighted retrieval proxy are shown. The lack of sensitivity for the polarimetric v_e retrieval above values of 0.11 is not physical but instead due to retrieval algorithm limitations.

correlation of the r_e(3.7 μm) retrieval bias with the value of v_e(2WT) in Figure 8c. This implies that distinguishing the impact of the bispectral v_e assumption from the accuracy of the vertical weighting assumptions could be problematic. The impact of the bispectral v_e assumption will be discussed further on in this section with regard to polarimetric retrievals of r_e and v_e.

The removal of the transition zone is assumed to isolate the core of the cloud from the region that could be influenced by cloud top entrainment. While a rigorous definition of this region requires characterization of both the dynamics and microphysics, it is outside the scope of this retrieval study to identify the dynamical causes of the transition zone. We have instead inferred the presence of this feature from the microphysical properties in the LES snapshots because of the clearly altered microphysics of this region. Resolving the transition zone in this manner can be complicated by the coarseness of the vertical resolution of the LES. This is especially true for the resolution of the ATEX cases where situations can occur such that the optical cloud top and transition zone base cannot be distinguished from one another. Thus, for the ATEX cases, the impact of the removal of the transition zone on the retrieval bias can only serve as a low estimate.

While this work has primarily focused on bispectral LWP retrievals, the core concept behind this passive retrieval technique is likely to be extended to future spaceborne polarimetric instruments. The work of *Alexandrov et al.* [2012] as well as our own polarimetric simulator studies in *Miller et al.* [2013] has demonstrated that vertically weighted retrieval proxies, [r_e(2WT), v_e(2WT)], compare well with polarimetric retrievals, [r_e(pol.), v_e(pol.)] Figures 9 and 10. The spatial distributions of all of the r_e microphysical retrieval techniques are shown in Figures 10a–10c. The similarities between r_e(2WT) and r_e(pol.) imply that polarimetric retrievals may exhibit a similar sensitivity to the removal of the transition zone. It follows that a cursory understanding of the impact of cloud vertical profile on polarimetric and spectral retrievals can be obtained from this study. For example, the comparison between the retrieval biases in Figures 6c and 8c may also imply that the

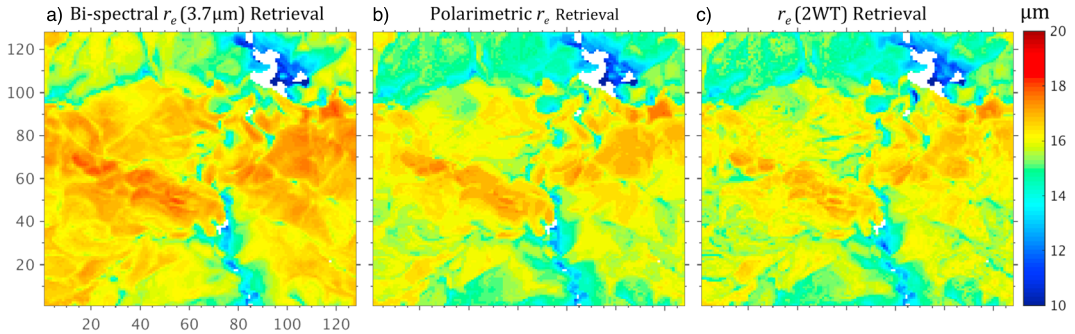

Figure 10. Droplet effective radius retrievals from the DYCOMS-II case for a variety of retrieval techniques. The retrievals displayed have been obtained using the (a) bispectral method, (b) the polarimetric method, and (c) the vertically weighted retrieval proxy.

standard deviation of the retrieval bias for r_e(pol.) would be much less than for r_e(3.7 μm). This difference in the accuracy of the retrieval bias occurs in part because r_e(2WT) and r_e(pol.) make no explicit assumption about the value of v_e. As the scatterplot in Figure 8c revealed, v_e(2WT) is correlated with the value of the r_e (3.7 μm) retrieval bias, and this correlation is also demonstrated spatially in the comparison of Figures 9a and 9c. This systematic broadening of the bias indicates that the bispectral assumption of $v_e = 0.1$ results in a lack of sensitivity to the removal of the transition zone. In contrast, the r_e(2WT)/polarimetric retrieval bias clearly improves after removing the transition zone. Thus, polarimetric retrievals of LWP may have to take into consideration the impact that the cloud top transition zone might have on retrieval quality. Further study on the sensitivity of polarimetric retrievals to the cloud top transition may be necessary for future polarimetric campaigns like those of NASA's upcoming Pre-Aerosol Clouds and ocean Ecosystem mission and ESA's Multiviewing Multichannel Multipolarization mission. It should be noted that for MODIS cloud products the bias due to the v_e assumption does not substantially impact the r_e retrieval compared to other sources of bias (i.e., cloud inhomogeneity or 3-D effects). In the MODIS Collection 6 cloud products, the uncertainty associated with the v_e assumption is included in the determination of the retrieval uncertainty data products.

6. Conclusions

The LES cloud retrieval simulator used in this study has allowed us to probe the impact of cloud vertical structure on passive LWP retrievals for marine boundary layer clouds in two regimes: trade wind cumulus and subtropical stratocumulus. With regard to the three questions that motivated this study we have found the following:

1. The vertical profile assumption (homogeneous or adiabatic) most appropriate for LWP retrieval depends on cloud regime (cumuliform or stratiform).
2. The vertical profiles of the LES cloud cases were quite varied, with some dominated by strong drizzle production and others by the microphysical impact of entrainment. Each of these features was found to bias LWP retrievals low, leading to a more favorable retrieval for homogeneous vertical profile assumptions.
3. The theoretical framework developed here defines LWP in terms of an arbitrary droplet vertical profile. This framework was used to demonstrate that the large variability in the bias of LWP retrievals was associated with varying vertical profiles of CDNC and droplet size distribution dispersion (both of which are assumed to be constant in the standard adiabatic profile).

A primary objective of this study was to identify the cloud vertical profile assumption most appropriate for LWP retrievals; however, we have found that simply asking which retrieval assumptions perform better is not a particularly fruitful approach to these issues. In fact, there is likely no such thing as an ideal retrieval assumption that suits all cloud regimes. With that in mind, the impact of the a priori cloud vertical profile assumption should not be neglected when attempting passive LWP retrievals. Future work needs to address a method of identifying appropriate a priori vertical profile assumptions by constraining them relative to other measureable or retrievable cloud properties.

The focus on high-resolution retrievals based on 1-D radiative transfer leaves questions for future studies. While these model choices were invoked to focus on biases associated with cloud vertical profile assumptions, it does limit the scope of this study. Future work will need to also identify the relative importance cloud vertical profile and cloud horizontal heterogeneity or 3-D radiative effects on retrievals. This study begins the discussion of a broader and more complicated study of the impact of cloud vertical profile on LWP retrievals when including all possible cloud retrieval biases.

The results of this study are not limited to the passive bispectral retrieval of LWP. Regardless of the microphysical retrieval technique, the profile assumption bias has an impact on any passive shortwave retrieval based on the retrieval relationship in equation (1). As we have demonstrated, polarimetric retrievals of droplet microphysics do not avoid this limitation. In fact, polarimetric retrievals exhibit a more acute sensitivity to the cloud top transition zone than bispectral retrievals. This is due, in part, to the influence of the bispectral v_e assumption on the variability of r_e retrievals. The r_e retrieval variability induced by this assumption is of the same magnitude as the impact of the transition zone. Future polarimetric microphysical retrievals, unencumbered by the v_e assumption will likely be sensitive to the cloud top transition zone, and this could in turn influence the future climatic record of LWP measurements.

Acknowledgments
This work was funded in part through NASA grants NNX11AR06G and NNX14AJ25G. The authors appreciate the continuing support of Hal Maring at NASA Headquarters. D.J.M. acknowledges the NASA Earth and Space Science Fellowship (NESSF) managed by Ming-Ying Wei. The hardware used in the computational studies is part of the UMBC High Performance Computing Facility (HPCF). The facility is supported by the U.S. National Science Foundation through the MRI program (grants CNS-0821258 and CNS-1228778) and the SCREMS program (grant DMS-0821311), with additional substantial support from the University of Maryland, Baltimore County (UMBC).

References

Ackerman, A. S., P. V. Hobbs, and O. B. Toon (1995), A model for particle microphysics, turbulent mixing, and radiative transfer in the stratocumulus-topped marine boundary layer and comparisons with measurements, *J. Atmos. Sci.*, *52*(8), 1204–1236.

Ackerman, A. S., M. P. Kirkpatrick, D. E. Stevens, and O. B. Toon (2004), The impact of humidity above stratiform clouds on indirect aerosol climate forcing, *Nature*, *432*(7020), 1014–1017.

Ackerman, A. S., et al. (2009), Large-eddy simulations of a drizzling, stratocumulus-topped marine boundary layer, *Mon. Weather Rev.*, *137*(3), 1083–1110, doi:10.1175/2008MWR2582.1.

Alexandrov, M. D., B. Cairns, C. Emde, A. S. Ackerman, and B. van Diedenhoven (2012), Remote sensing of environment, *Remote Sens. Environ.*, *125*(C), 92–111, doi:10.1016/j.rse.2012.07.012.

Baker, M. B., and J. Latham (1979), The evolution of droplet spectra and the rate of production of embryonic raindrops in small cumulus clouds, *J. Atmos. Sci.*, *36*(8), 1612–1615, doi:10.1175/1520-0469(1979)036<1612:TEODSA>2.0.CO;2.

Bennartz, R. (2007), Global assessment of marine boundary layer cloud droplet number concentration from satellite, *J. Geophys. Res.*, *112*, D02201, doi:10.1029/2006JD007547.

Boers, R., J. R. Acarreta, and J. L. Gras (2006), Satellite monitoring of the first indirect aerosol effect: Retrieval of the droplet concentration of water clouds, *J. Geophys. Res.*, *111*, D22208, doi:10.1029/2005JD006838.

Brenguier, J. L., F. Burnet, and O. Geoffroy (2011), Cloud optical thickness and liquid water path—Does the *k* coefficient vary with droplet concentration? *Atmos. Chem. Phys.*, *11*(18), 9771–9786, doi:10.5194/acp-11-9771-2011.

Brenguier, J.-L., H. Pawlowska, and L. Schüller (2003), Cloud microphysical and radiative properties for parameterization and satellite monitoring of the indirect effect of aerosol on climate, *J. Geophys. Res.*, *108*(D), 8632, doi:10.1029/2002JD002682.

Cho, H. M., et al. (2015), Frequency and causes of failed MODIS cloud property retrievals for liquid phase clouds over global oceans, *J. Geophys. Res. Atmos.*, *120*, 4132–4154, doi:10.1002/2015JD023161.

Costantino, L., and F. M. Breon (2013), Aerosol indirect effect on warm clouds over South-East Atlantic, from co-located MODIS and CALIPSO observations, *Atmos. Chem. Phys.*, *13*(1), 69–88, doi:10.5194/acp-13-69-2013.

Fridlind, A. M., and A. S. Ackerman (2011), Estimating the sensitivity of radiative impacts of shallow, broken marine clouds to boundary layer aerosol size distribution parameter uncertainties for evaluation of satellite retrieval requirements, *J. Atmos. Oceanic Technol.*, *28*(4), 530–538, doi:10.1175/2010JTECHA1520.1.

Jiang, J. H., et al. (2012), Evaluation of cloud and water vapor simulations in CMIP5 climate models using NASA "A-Train" satellite observations, *J. Geophys. Res.*, *117*, D14105, doi:10.1029/2011JD017237.

King, M. D., W. P. Menzel, Y. J. Kaufman, D. Tanré, B.-C. Gao, S. Platnick, S. A. Ackerman, L. A. Remer, R. Pincus, and P. A. Hubanks (2003), Cloud and aerosol properties, precipitable water, and profiles of temperature and water vapor from MODIS, *IEEE Trans. Geosci. Remote Sens.*, *41*(2), 442–458, doi:10.1109/TGRS.2002.808226.

Kubar, T. L., and D. L. Hartmann (2009), Understanding the importance of microphysics and macrophysics for warm rain in marine low clouds. Part II: Heuristic models of rain formation, *J. Atmos.*, *66*, 2953–2972, doi:10.1175/2009JAS3071.1.

Lebsock, M., and H. Su (2014), Application of active spaceborne remote sensing for understanding biases between passive cloud water path retrievals, *J. Geophys. Res. Atmos.*, 8962–8979, doi:10.1002/2014JD021568.

Marshak, A., S. Platnick, T. Várnai, G. Wen, and R. F. Cahalan (2006), Impact of three-dimensional radiative effects on satellite retrievals of cloud droplet sizes, *J. Geophys. Res.*, *111*, D09207, doi:10.1029/2005JD006686.

Miles, N. L., J. Verlinde, and E. E. Clothiaux (2000), Cloud droplet size distributions in low-level stratiform clouds, *J. Atmos. Sci.*, *57*(2), 295–311, doi:10.1175/1520-0469(2000)057<0295:CDSDIL>2.0.CO;2.

Miller, D. J., Z. Zhang, S. Platnick, A. S. Ackerman, C. Cornet, B. A. Baum (2013), Exploring the effects of cloud vertical and horizontal structure on cloud microphysics retrievals based on polarized reflectances, presented at the *2013 AGU Fall Meeting*, San Francisco, doi:10.13140/2.1.2948.7043.

Nakajima, T., and M. D. King (1990), Determination of the optical thickness and effective particle radius of clouds from reflected solar radiation measurements. Part I: Theory, *J. Atmos. Sci.*, *47*(15), 1878–1893, doi:10.1175/1520-0469(1990)047<1878:dotota>2.0.co;2.

Nicholls, S., and J. Leighton (1986), An observational study of the structure of stratiform cloud sheets: Part I. Structure, *Q. J. R. Meteorol. Soc.*, *112*(472), 431–460, doi:10.1002/qj.49711247209.

Noble, S. R., and J. G. Hudson (2015), MODIS comparisons with northeastern Pacific in situ stratocumulus microphysics, *J. Geophys. Res. Atmos.*, *120*, 8332–8344, doi:10.1002/2014JD022785.

Oreopoulos, L., and R. Davies (1998), Plane parallel albedo biases from satellite observations. Part I: Dependence on resolution and other factors, *J. Clim.*, *11*(5), 919–932.

Platnick, S. (2000), Vertical photon transport in cloud remote sensing problems, *J. Geophys. Res.*, *105*(D18), 22,919–22,935, doi:10.1029/2000JD900333.

Platnick, S., M. D. King, S. A. Ackerman, W. P. Menzel, B. A. Baum, J. C. Riedi, and R. A. Frey (2003), The MODIS cloud products: Algorithms and examples from terra, *IEEE Trans. Geosci. Remote Sens.*, *41*(2), 459–473, doi:10.1109/TGRS.2002.808301.

Pontikis, C. A. (1996), Parameterization of the droplet effective radius of warm layer clouds, *Geophys. Res. Lett.*, *23*(19), 2629–2632, doi:10.1029/96GL02452.

Pontikis, C. A., and E. M. Hicks (1993), Droplet activation as related to entrainment and mixing in warm tropical maritime clouds, *J. Atmos. Sci.*, *50*(13), 1888–1896, doi:10.1175/1520-0469(1993)050<1888:DAARTE>2.0.CO;2.

Roebeling, R. A., A. J. Feijt, and P. Stammes (2006), Cloud property retrievals for climate monitoring: Implications of differences between Spinning Enhanced Visible and Infrared Imager (SEVIRI) on METEOSAT-8 and advanced very high resolution radiometer (AVHRR) on NOAA-17, *J. Geophys. Res.*, *111*, D20210, doi:10.1029/2005JD006990.

Rosenfeld, D., G. Liu, X. Yu, Y. Zhu, and J. Dai (2014), High-resolution (375 m) cloud microstructure as seen from the NPP/VIIRS satellite imager, *Atmos. Chem. Phys.*, *14*, 2479–2496, doi:10.5194/acp-14-2479-2014.

Seethala, C., and Á. Horváth (2010), Global assessment of AMSR-E and MODIS cloud liquid water path retrievals in warm oceanic clouds, *J. Geophys. Res.*, *115*, D13202, doi:10.1029/2009JD012662.

Stamnes, K., S.-C. Tsay, W. Wiscombe, and K. Jayaweera (1988), Numerically stable algorithm for discrete-ordinate-method radiative transfer in multiple scattering and emitting layered media, *Appl. Opt.*, *27*(12), 2502–2509, doi:10.1364/AO.27.002502.

Stevens, B., A. S. Ackerman, B. A. Albrecht, A. R. Brown, A. Chlond, J. Cuxart, P. G. Duynkerke, D. C. Lewellen, M. K. Macvean, and R. A. J. Neggers (2001), Simulations of trade wind cumuli under a strong inversion, *J. Atmos. Sci.*, *58*(14), 1870–1891, doi:10.1175/1520-0469(2001)058<1870:SOTWCU>2.0.CO;2.

Stevens, B., et al. (2003), Dynamics and Chemistry of Marine Stratocumulus—DYCOMS-II, *Am. Meteorol. Soc.*, doi:10.1175/BAMS-84-5-579.

Stevens, B., et al. (2005), Evaluation of large-eddy simulations via observations of nocturnal marine stratocumulus, *Mon. Weather Rev.*, *133*(6), 1443–1462, doi:10.1175/MWR2930.1.

Suzuki, K., G. L. Stephens, S. C. van den Heever, and T. Y. Nakajima (2011), Diagnosis of the warm rain process in cloud-resolving models using joint CloudSat and MODIS observations, *Am. Meteorol. Soc.*, doi:10.1175/JAS-D-10-05026.1.

Szczodrak, M., P. H. Austin, and P. B. Krummel (2001), Variability of optical depth and effective radius in marine stratocumulus clouds, *J. Atmos. Sci.*, *58*(19), 2912–2926, doi:10.1175/1520-0469(2001)058<2912:VOODAE>2.0.CO;2.

Várnai, T., and A. Marshak (2001), Statistical analysis of the uncertainties in cloud optical depth retrievals caused by three-dimensional radiative effects, *J. Atmos. Sci.*, *58*(12), 1540–1548, doi:10.1175/1520-0469(2001)058<1540:SAOTUI>2.0.CO;2.

Várnai, T., and A. Marshak (2002), Observations of three-dimensional radiative effects that influence MODIS cloud optical thickness retrievals, *J. Atmos. Sci.*, *59*(9), doi:10.1175/1520-0469(2002)059<1607:OOTDRE>2.0.CO;2.

Várnai, T., and R. Davies (1999), Effects of cloud heterogeneities on shortwave radiation: Comparison of cloud-top variability and internal heterogeneity, *J. Atmos. Sci.*, *56*(24), 4206–4224, doi:10.1175/1520-0469(1999)056<4206:EOCHOS>2.0.CO;2.

Wood, R., and D. L. Hartmann (2006), Spatial variability of liquid water path in marine low cloud: The importance of mesoscale cellular convection, *J. Clim.*, *19*(9), 1748–1764, doi:10.1175/JCLI3702.1.

Zhang, Z., and S. Platnick (2011), An assessment of differences between cloud effective particle radius retrievals for marine water clouds from three MODIS spectral bands, *J. Geophys. Res.*, *116*, D20215, doi:10.1029/2011JD016216.

Zhang, Z., A. S. Ackerman, G. Feingold, S. Platnick, R. Pincus, and H. Xue (2012), Effects of cloud horizontal inhomogeneity and drizzle on remote sensing of cloud droplet effective radius: Case studies based on large-eddy simulations, *J. Geophys. Res.*, *117*, D19208, doi:10.1029/2012JD017655.